

Second-harmonic generation and linear electro-optical coefficients of SiC polytypes and nanotubes

I. J. Wu and G. Y. Guo*

*Department of Physics and Center for Theoretical Sciences,
National Taiwan University, Taipei, Taiwan 106, Republic of China*

(Dated: October 23, 2018)

The second-order nonlinear optical susceptibility ($\chi_{abc}^{(2)}$) and linear electro-optical coefficient (r_{abc}) of a large number of single-walled zigzag, armchair and chiral SiC nanotubes (SiC-NTs) as well as bulk SiC polytypes (2H-, 4H-, 6H- and 3C-SiC) and single graphitic SiC sheet have been calculated from first-principles. The calculations are based on density functional theory in the local density approximation and highly accurate full-potential projector augmented-wave method is used. Both the zigzag and chiral SiC-NTs are found to exhibit large second-order nonlinear optical behavior with the $\chi_{abc}^{(2)}$ and r_{abc} coefficients being up to ten-times larger than that of bulk SiC polytypes, and also being up to thirteen-times larger than the counterparts of the corresponding BN-NTs, indicating that SiC-NTs are promising materials for nonlinear optical and opto-electric applications. The prominent features in the spectra of $\chi_{abc}^{(2)}(-2\omega, \omega, \omega)$ of the SiC-NTs are correlated with the features in the linear optical dielectric function $\varepsilon(\omega)$ in terms of single-photon and two-photon resonances.

PACS numbers: 42.65.-k, 42.70.Nq, 73.22.-f, 78.67.Ch

I. INTRODUCTION

Carbon nanotubes (CNTs) have attracted considerable interest worldwide ever since their discovery in 1991 [1], mainly because of their unusual properties and great potentials for technological applications. CNTs can be regarded as a layer of graphene sheet rolled up in a tubular form [2], and the structure of a CNT is specified by a chiral vector defined by a pair of integers (n, m) . CNTs can be chiral or nonchiral depending on the way they are rolled up. Their physical properties, in particular, optical dielectric functions, depend sensitively on their chirality, i.e., the (n, m) indices (see, e.g., Refs. 3 and 4 and references therein). Apart from CNTs, inorganic tubular materials, such as BN [5, 6], AlN [7], GaN [8], have also been predicted and synthesized. These tubular materials also display some very interesting properties distinctly different from their bulks.

Bulk silicon carbide (SiC) crystallizes in either a cubic or a hexagonal form, and exhibits polytypism [9, 10]. The polytypes are made of identical hexagonal layers with different stacking sequences. These polytypes are semiconductors with a range of band gaps, from 2.39 eV in the zincblende (3C) to 3.33 eV in the wurtzite polytype (2H) [9, 11]. Furthermore, 3C- and 6H-SiC are used for high temperature, high-power and high-frequency devices [12, 13, 14, 15] due to their unique properties [16], while 6H-SiC with a band gap of 2.86 eV is a useful material for blue light-emitting diode applications [11]. Recently, SiC-NTs were also synthesized by the reaction of CNTs and SiO at different temperatures [17]. This has stimulated a number of theoretical and experimental investigations on the tubular form of

the SiC [18, 19, 20, 21, 22]. Based on density-functional calculations, Miyamoto and Yu [23] predicted the existence of graphitic and tubular forms of SiC and also proposed their synthesis using an extreme hole injection technique. They also reported that the strain energies of SiC-NTs are lower than that of CNTs, and that the band gaps of SiC-NTs can be direct or indirect, depending on the chirality. Using both tight-binding molecular dynamics and *ab initio* methods, Menon and coworkers [20] showed that single-walled SiC-NTs are highly stable with a large band gap. Zhao *et al.* [24] also investigated theoretically the strain energy, atomic and electronic structure of SiC-NTs with or without hydrogenation. Gali performed an *ab initio* study of the effect of nitrogen and boron impurities on the band structure of the SiC-NTs [25].

Unlike CNTs, SiC-NTs are polar materials and therefore, may exhibit some unusual physical properties that CNTs may not have. For example, like BN-NTs, [26, 27] zigzag SiC-NTs may become piezoelectric, and also show second-order non-linear optical response. Despite the intensive theoretical studies mentioned above, no *ab initio* calculation of the dielectric response and optical properties of SiC-NTs has been reported, perhaps because of the heavy demand on computer resources. A knowledge of the optical properties of SiC-NTs is important for their optical and electrooptical applications. Therefore, we have recently carried out a series of *ab initio* calculations in order to analyze the linear optical features and underlying band structure of all three types of the SiC-NTs as well as their possible dependence on diameter and chirality. [28] In this work, we investigate the second-order optical susceptibility and also linear electro-optical coefficient of the SiC-NTs as well as bulk SiC polytypes. The primary objective of this work is to find out the features and magnitude of the second-harmonic generation and linear electro-optical coefficients of the SiC-NTs in or-

*Electronic address: gyguo@phys.ntu.edu.tw

der to see whether they have any potential applications in nonlinear optical and electro-optical devices such as second-harmonic generation, sum-frequency generation, and electrical optical switch. The second objective is to identify distinguished differences in nonlinear optical properties between SiC-NTs and CNTs [3], and also between SiC-NTs and BN-NTs [27].

The rest of this paper is organized as follows. In Sec. II, the theoretical approach and computational method are described. In Sec. III, the calculated second-order nonlinear optical susceptibility and linear electro-optical coefficients of SiC nanotubes are presented. For comparison, the second-order nonlinear optical susceptibility and linear electro-optical coefficients of bulk SiC polytypes and single graphitic SiC sheet are also calculated and presented. Finally, in Sec. IV, a summary is given.

II. THEORY AND COMPUTATIONAL METHOD

Our *ab initio* calculations for the SiC-NTs were performed using highly accurate full-potential projector augmented-wave (PAW) method [29], as implemented in the vasp package [30]. They are based on density functional theory (DFT) with the local density approximation (LDA). A supercell geometry was adopted so that the nanotubes are aligned in a square array with the closest distance between adjacent nanotubes being at least 10 Å. A large plane-wave energy cutoff of 450 eV was used throughout. We consider a large number of representative SiC-NTs with a range of diameters from all three types, as listed in Ref. 28.

First, the ideal nanotubes were constructed by rolling-up a hexagonal SiC sheet. The atomic positions and lattice constants were then fully relaxed by the conjugate gradient technique. The theoretical equilibrium atomic positions and lattice constant were obtained when the forces acting on all the atoms and the uniaxial stress were less than 0.04 eV/Å and 1.0 kBar, respectively. The calculated equilibrium lattice constants T and curvature energies E_c (total energy relative to that of single SiC sheet) as well as the other computational details have been reported before [28].

The final self-consistent electronic band structure calculations were then carried out for the theoretically determined SiC-NT structures. In this work, the nonlinear optical properties were calculated based on the independent-particle approximation, i.e., the excitonic effects and the local-field corrections were neglected. Note that the band gap of SiC in the wurtzite (2H) structure from our LDA calculations is 2.12 eV (see Sec. IIIA below), being 1.18 eV smaller than the experimental value [9, 11]. This suggests that the quasi-particle self-energy corrections to the optical peak positions may amount to ~ 1 eV in the SiC systems. Furthermore, because the LDA underestimates the energy gaps, the calculated dielectric function and second-order nonlinear

optical susceptibility in the static limit might be slightly too large in general. For example, our calculated dielectric function at 0 eV for the electric field parallel and perpendicular to the c -axis of 2H-SiC is 8.33 and 7.90, respectively, being slightly larger than the corresponding measured ϵ_∞ , 6.84 and 6.51. [9] Therefore, the results from the present LDA-independent-particle calculations might not be able to be compared quantitatively with experiments, though they would certainly be useful to study the trends and characteristics of the optical properties of the SiC-NTs. Nonetheless, our previous calculations show that the dielectric functions of graphite [3] and also of h-BN [27] calculated within the independent-particle picture are in reasonable agreement with experiments, perhaps because of the accidental cancellation of the self-energy corrections by the excitonic effects.

Following previous nonlinear optical calculations [3, 27, 31], the imaginary part of the second-order optical susceptibility due to direction interband transitions is given by [32]

$$\chi_{abc}^{(2)}(-2\omega, \omega, \omega) = \chi_{abc,VE}^{(2)}(-2\omega, \omega, \omega) + \chi_{abc,VH}^{(2)}(-2\omega, \omega, \omega) \quad (1)$$

where the contribution due to the so-called virtual-electron (VE) process is

$$\chi_{abc,VE}^{(2)} = -\frac{\pi}{2\Omega} \sum_{i \in VB} \sum_{j,l \in CB} \sum_{\mathbf{k}} w_{\mathbf{k}} \left\{ \frac{Im[p_{jl}^a \langle p_{li}^b p_{ij}^c \rangle]}{\epsilon_{li}^3(\epsilon_{li} + \epsilon_{ji})} \delta(\epsilon_{li} - \omega) - \frac{Im[p_{ij}^a \langle p_{jl}^b p_{li}^c \rangle]}{\epsilon_{li}^3(2\epsilon_{li} - \epsilon_{ji})} \delta(\epsilon_{li} - \omega) + \frac{16Im[p_{ij}^a \langle p_{jl}^b p_{li}^c \rangle]}{\epsilon_{ji}^3(2\epsilon_{li} - \epsilon_{ji})} \delta(\epsilon_{ji} - 2\omega) \right\} \quad (2)$$

and that due to the virtual-hole (VH) process

$$\chi_{abc,VH}^{(2)} = \frac{\pi}{2\Omega} \sum_{i,l \in VB} \sum_{j \in CB} \sum_{\mathbf{k}} w_{\mathbf{k}} \left\{ \frac{Im[p_{li}^a \langle p_{ij}^b p_{jl}^c \rangle]}{\epsilon_{jl}^3(\epsilon_{jl} + \epsilon_{ji})} \delta(\epsilon_{jl} - \omega) - \frac{Im[p_{ij}^a \langle p_{jl}^b p_{li}^c \rangle]}{\epsilon_{ji}^3(2\epsilon_{jl} - \epsilon_{ji})} \delta(\epsilon_{jl} - \omega) + \frac{16Im[p_{ij}^a \langle p_{jl}^b p_{li}^c \rangle]}{\epsilon_{ji}^3(2\epsilon_{jl} - \epsilon_{ji})} \delta(\epsilon_{ji} - 2\omega) \right\} \quad (3)$$

Here $\epsilon_{ji} = \epsilon_{\mathbf{k}j} - \epsilon_{\mathbf{k}i}$ and $\langle p_{jl}^b p_{li}^c \rangle = \frac{1}{2}(p_{jl}^b p_{li}^c + p_{li}^b p_{jl}^c)$. The dipole transition matrix elements $p_{ij}^a = \langle \mathbf{k}j | \hat{p}_a | \mathbf{k}i \rangle$ were obtained from the self-consistent band structures within the PAW formalism [33]. The real part of the second-order optical susceptibility is then obtained from $\chi_{abc}^{(2)}$ by a Kramer-Kronig transformation

$$\chi^{(2)}(-2\omega, \omega, \omega) = \frac{2}{\pi} \mathbf{P} \int_0^\infty d\omega' \frac{\omega' \chi''^{(2)}(2\omega', \omega', \omega')}{\omega'^2 - \omega^2}. \quad (4)$$

The linear electro-optic coefficient $r_{abc}(\omega)$ is connected to the second-order optical susceptibility $\chi_{abc}^{(2)}(-\omega, \omega, 0)$ through the relation [34]

$$\chi_{abc}^{(2)}(-\omega, \omega, 0) = -\frac{1}{2} n_a^2(\omega) n_b^2(\omega) r_{abc}(\omega) \quad (5)$$

where $n_a(\omega)$ is the refraction index in the a -direction. In the zero frequency limit,

$$\lim_{\omega \rightarrow 0} \chi_{abc}^{(2)}(-2\omega, \omega, \omega) = \lim_{\omega \rightarrow 0} \chi_{abc}^{(2)}(-\omega, \omega, 0). \quad (6)$$

Therefore,

$$r_{abc}(0) = -\frac{2}{n_a^2(0)n_b^2(0)} \lim_{\omega \rightarrow 0} \chi_{abc}^{(2)}(-2\omega, \omega, \omega). \quad (7)$$

Furthermore, for the photon energy $\hbar\omega$ well below the band gap, the linear electro-optic coefficient $r_{abc}(\omega) \approx r_{abc}(0)$ because $\chi_{abc}^{(2)}(-2\omega, \omega, \omega)$ and $n(\omega)$ are nearly constant in this low frequency region, as shown in the next section and in Ref. [28].

In the present calculations, the δ -function in Eqs. (2)-(3) is approximated by a Gaussian function with $\Gamma = 0.2$ eV. A uniform k -point grid ($1 \times 1 \times n$) along the nanotube axis (z -axis) with the number n being from 40 to 100, is used. Furthermore, to ensure that $\chi_{abc}^{(2)}$ calculated via Kramer-Kronig transformation (Eq. (4)) is reliable, at least ten energy bands per atom are included in the present optical calculations. The unit cell volume Ω in Eqs. (2)-(3) is not well defined for nanotubes. Therefore, like the previous calculations [3, 4, 27, 28], we used the effective unit cell volume of the nanotubes rather than the volume of the supercells which is arbitrary. The effective unit cell of a nanotube is given by $\Omega = \pi[(D/2 + d/2)^2 - (D/2 - d/2)^2]T = \pi DdT$ where d is the thickness of the nanotube cylinder which is set to the interlayer distance of h -SiC (3.51 Å [28]). D and T are the diameter and length of translational vector of the nanotube [28], respectively.

III. RESULTS AND DISCUSSION

A. Bulk SiC polytypes

For comparison with the SiC-NTs, we first investigated the second-order nonlinear optical susceptibility of bulk SiC polytypes. SiC exists in either a cubic or a hexagonal polymorphic structure. The polytypes are made of identical hexagonal layers with different stacking sequences. SiC occurs in nearly 200 polytypes.[35] Here we consider only the four common 2H, 4H, 6H and 3C types of SiC. The zincblende (3C) structure, with pure cubic stacking of the Si-C double layers in the [111] direction, is one of the two most extreme polytypes. The other is the wurtzite (2H) structure with pure hexagonal stacking in the [0001] direction. The atomic positions and lattice constants of the four polytypes were theoretically optimized. In the atomic structure optimizations, a uniform k -point grid of $30 \times 30 \times n$ with n being from 15 to 30 was used. The calculated equilibrium lattice constants of the SiC polytypes are listed in Table I, together with previous theoretical and experimental values. Table I shows that our theoretical lattice constants are in very good agreement with the previous calculations [36], though they are slightly smaller (within 0.7 %) than the corresponding experimental values [9]. Our calculated indirect band gaps for the 3C, 2H, 4H and 6H types of SiC are, respectively, 1.29 eV, 2.12 eV, 2.17 eV and 1.96 eV. These

band gap values are smaller by about 1.1 eV than the corresponding experimental values [9] of 2.39 (3C), 3.33 eV (2H), 3.26 eV (4H), and 2.86 eV (6H). Nonetheless, our theoretical band gap values are in very good agreement with previous LDA calculations (see, e.g., Ref. 37 and references therein). The difference in the theoretical DFT-LDA and experimental band gap values can be attributed to the quasi-particle self-energy corrections, as has been shown explicitly in previous quasiparticle band structure calculations for the SiC polytypes [37].

In Fig. 1, we display the imaginary and real parts of three nonvanishing components of the second-order nonlinear optical susceptibility (tensor) $\chi^{(2)}(-2\omega, \omega, \omega)$ of the three hexagonal SiC polytypes. The imaginary and real parts of the nonvanishing component $\chi_{xyz}^{(2)}(-2\omega, \omega, \omega)$ of the cubic SiC are plotted in Fig. 2. In the nonlinear optical calculations, we used a denser k -point grid of $50 \times 50 \times n$ with n being from 10 to 30 for the three hexagonal SiC polytypes, and $n = 50$ for the cubic SiC. Importantly, we find numerically that only the $\chi_{zzz}^{(2)}$, $\chi_{zxx}^{(2)}$, $\chi_{zyy}^{(2)}$, $\chi_{xzz}^{(2)}$, $\chi_{yzy}^{(2)}$, $\chi_{xxz}^{(2)}$, and $\chi_{yyz}^{(2)}$ components are nonzero for the three hexagonal polytypes. Moreover, $\chi_{zyy}^{(2)} = \chi_{zxx}^{(2)}$, and $\chi_{yyz}^{(2)} = \chi_{xxz}^{(2)} = \chi_{xzx}^{(2)} = \chi_{yzy}^{(2)}$. This is consistent with the symmetry consideration, [38] demonstrating that our numerical method and calculations are qualitatively correct. For the 3C-SiC, only $\chi_{xyz}^{(2)}$, $\chi_{zxx}^{(2)}$, $\chi_{yzz}^{(2)}$ components are nonzero, and all the three components are numerically found to be identical, as they should. Fig. 1 shows that the line shape, amplitude and feature positions of the $\chi_{zxx}^{(2)}$ and $\chi_{xzz}^{(2)}$ components for all the hexagonal SiC polytypes are very similar. On the other hand, the $\chi_{zzz}^{(2)}$ component varies significantly as one moves from 2H- to 6H-SiC. This is mainly because in this case all the electric fields are polarized parallel to the z -axis and hence the $\chi_{zzz}^{(2)}$ component should be rather sensitive to the layer stacking sequence along the z -axis. We also note that the shape of the $\chi_{xyz}^{(2)}$ of 3C SiC is similar to that of the $\chi_{zzz}^{(2)}$ of 6H-SiC (Fig. 1 and Fig. 2). Nonetheless, the features in the $\chi_{xyz}^{(2)}$ of the cubic structure appears to have the largest magnitude among the four SiC polytypes studied here.

We find that our calculated nonzero components of $\chi^{(2)}(-2\omega, \omega, \omega)$ of all the four polytypes agree quite well with the recent DFT-LDA calculations by Adolph and Bechstedt [39]. For detailed comparison, we plot the imaginary part of the nonzero components of SiC in the cubic and wurtzite structures from the previous calculations by Adolph and Bechstedt [39] in Fig. 2 (cubic) and Fig. 3 (wurtzite), together with our results. One can see from Figs. 2 and 3(c) that $\chi_{xyz}^{(2)}(-2\omega, \omega, \omega)$ of 3C-SiC and $\chi_{xzx}^{(2)}(-2\omega, \omega, \omega)$ of 2H-SiC from the present and previous calculations are almost identical. Nonetheless, there are some discernable discrepancies in the $\chi_{zxx}^{(2)}$ and $\chi_{zzz}^{(2)}$ components of 2H-SiC between the two calculations [Fig. 3(a-b)].

TABLE I: Calculated lattice constants of SiC polytypes, together with other theoretical (Cal.) (Bechstedt *et al.* [36]) and experimental (Exp.) (Ref. 9) lattice constants.

	2H	4H	6H	3C
	a (Å), c (Å)	a (Å), c (Å)	a (Å), c (Å)	a (Å)
This work	3.057, 5.018	3.060, 10.018	3.061, 15.018	4.331
Cal.	3.057, 5.016	3.061, 10.012	3.062, 15.012	4.332
Exp.	3.076, 5.048	3.073, 10.053	3.081, 15.117	4.360

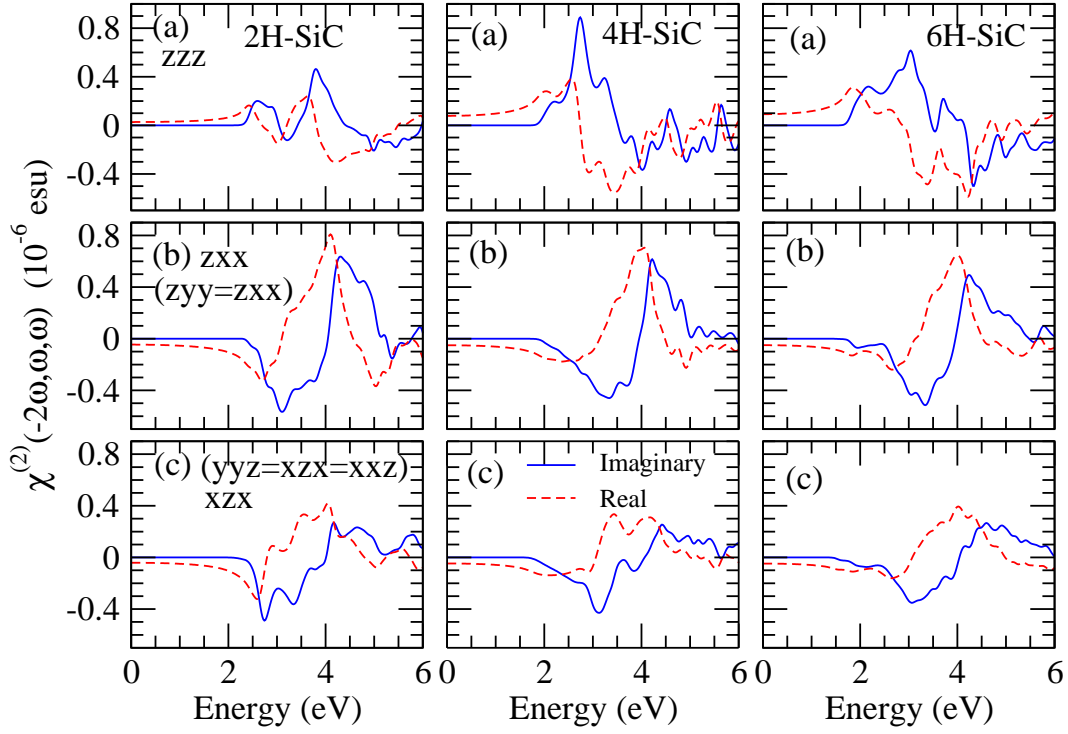


FIG. 1: (Color online) Real and imaginary parts of $\chi^{(2)}(-2\omega, \omega, \omega)$ of the hexagonal SiC polytypes.

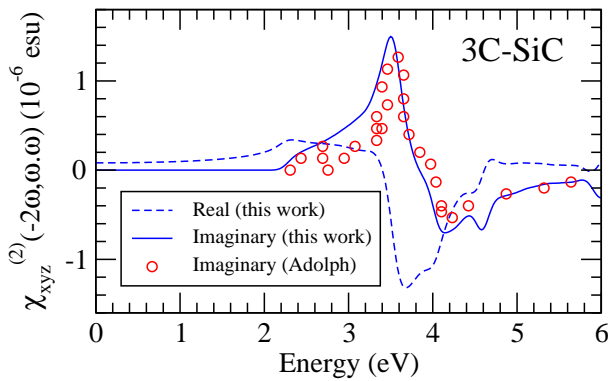


FIG. 2: (Color online) Real and imaginary parts of $\chi^{(2)}(-2\omega, \omega, \omega)$ of SiC in the zinc-blende (3C) structure. Previous calculations by Adolph *et al.* [39] are also displayed for comparison.

In Table II, the calculated zero frequency linear electro-optic coefficient $r(0)$ as well as the corresponding second-

TABLE II: Calculated static refraction index n , second-order optical susceptibility $\chi^{(2)}(0)$ (pm/V) and linear electro-optical coefficient r_{abc} (pm/V) of the hexagonal SiC polytypes (a), zinc-blende SiC (b) and also isolated SiC sheet (c).

(a)	n_x (n_z)	$\chi_{zzz}^{(2)}, \chi_{zxx}^{(2)}$	r_{zzz}, r_{zxx}
2H-SiC	2.81 (2.88)	11.5, -17.9	-0.33, 0.55
4H-SiC	2.83 (2.87)	32.8, -20.4	-0.97, 0.62
6H-SiC	2.82 (2.89)	38.6, -20.4	-1.11, 0.61
(b)	n	$\chi_{xyz}^{(2)}$	r_{xyz}
3C-SiC	2.95	34.2	-0.90
(c)	n_a (n_c)	$\chi_{bbb}^{(2)}, \chi_{aab}^{(2)}$	r_{bbb}, r_{aab}
SiC sheet	3.19 (2.01)	227.8, -227.8	-11.08, 11.08

order nonlinear optical susceptibility $\chi^{(2)}(0, 0, 0)$ are listed. The $r(0)$ is calculated from the corresponding $\chi^{(2)}(0, 0, 0)$ by using Eq. (7). We find that the calculated $\chi_{xzx}^{(2)}(0)$ and $\chi_{zxx}^{(2)}(0)$ for the three hexagonal SiC

polytypes differs slightly from each other, i.e., only approximately satisfying the requirement of the Kleiman symmetry [40]. In Table II, therefore, the $\chi_{zxx}^{(2)}(0)$ is listed as the averaged value of $\chi_{xzxx}^{(2)}(0)$ and $\chi_{zxzx}^{(2)}(0)$, and hence $r_{zxx}(0)$ as the averaged value of $r_{xzxx}(0)$ and $r_{zxzx}(0)$, for all the hexagonal SiC polytypes. Clearly, Table II shows that $\chi_{zxx}^{(2)}(0)$ and hence $r_{zxx}(0)$ are nearly the same for all the hexagonal SiC polytypes. In contrast, $\chi_{zzz}^{(2)}(0)$ and hence $r_{zzz}(0)$ increases substantially as one moves from 2H-SiC to 6H-SiC, suggesting that $\chi_{zzz}^{(2)}(0)$ and $r_{zzz}(0)$ are more sensitive to the layer stacking sequence along the z -axis. This may be expected since all the electric fields are polarized parallel to the z -axis in the latter case.

Our calculated nonvanishing components of $\chi^{(2)}(0)$ for the four polytypes are compared with previous *ab initio* calculations [39, 41, 42] and available experiments [43, 44] in Table III. Clearly, our results agree rather well with the previous *ab initio* calculations by Chen *et al.* [42]. Nonetheless, both the results of ours and of Chen *et al.* [42] appear to be nearly two-times larger than the previous *ab initio* calculations by Adolph *et al.* [39] and Rashkev *et al.* [41]. This is surprising since the imaginary parts of $\chi^{(2)}$ from both the present and previous [39] calculations are very similar (Figs. 2 and 3). The precise origin of these discrepancies is not known at moment. Finally, we would consider that the agreement between our results and the experimental values is rather good (Table III), given the large uncertainties in the available experimental data. [43, 44]

B. Single graphitic SiC sheet

In order to understand the nonlinear optical properties of the SiC-NTs, we have also calculated the second-order nonlinear optical susceptibilities for an isolated honeycomb SiC sheet. The isolated SiC sheet is simulated by a slab-super-cell approach with an intersheet distance of about 10 Å. The underlying structure was determined theoretically by using k -mesh of $100 \times 100 \times 1$, and the theoretical lattice constant is $a = 3.069$ Å. Interestingly, we find numerically that the $\chi_{aab}^{(2)}$, $\chi_{baa}^{(2)}$ and $\chi_{bbb}^{(2)}$ for the isolated SiC sheet are nonzero. Here a and b denote the two Cartesian coordinates within the SiC layer. Moreover, $\chi_{baa}^{(2)} = \chi_{aab}^{(2)}$ and $\chi_{bbb}^{(2)} = -\chi_{aab}^{(2)}$. This is consistent with the symmetry consideration, demonstrating again that our numerical method and calculations are qualitatively correct. It is because that the isolated SiC sheet does not have the spatial inversion symmetry (D_{6h}^4) and its symmetry class is D_{3h} ($P\bar{6}m2$). Therefore, the isolated SiC sheet has nonzero $\chi_{aab}^{(2)}$, $\chi_{baa}^{(2)}$ and $\chi_{bbb}^{(2)}$ from the symmetry consideration. [38]

We show in Fig. 4 the calculated real and imaginary parts as well as the absolute value of the imaginary part of $\chi_{aab}^{(2)}(-2\omega, \omega, \omega)$ of the single SiC sheet. It is clear from

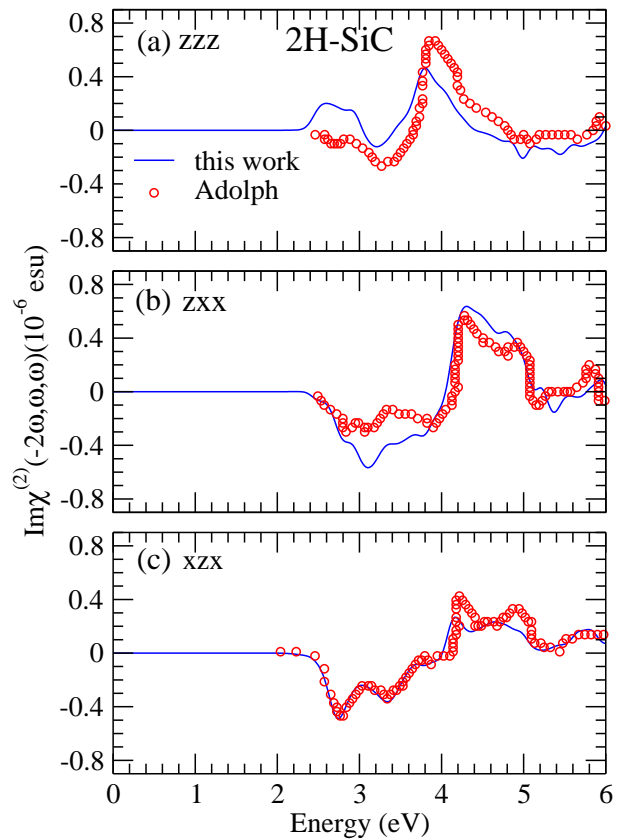


FIG. 3: (Color online) Imaginary parts of $\chi^{(2)}(-2\omega, \omega, \omega)$ of SiC in the wurtzite (2H) structure. Previous calculations by Adolph *et al.* [39] are also displayed for comparison.

Fig. 4 that the second harmonic generation (SHG) coefficient $\chi_{aab}^{(2)}(-2\omega, \omega, \omega)$ is significant in the entire range of the optical photon energy ($\hbar\omega$). Furthermore, for the photon energy smaller than about 1.2 eV, the $\chi_{aab}^{(2)}$ is purely dispersive (i.e., real and lossless) [Fig. 4(a)], suggesting that the SiC sheet has potential application in nonlinear optical devices. Note that since the SiC sheet has a theoretical band gap (E_g) of ~ 2.6 eV, the absorptive (imaginary) part of the $\chi_{aab}^{(2)}$ becomes zero below the half of the band gap (i.e., ~ 1.2 eV). The real part of the $\chi_{aab}^{(2)}$ remains nearly constant at low photon energies up to 0.5 eV, then increases steadily in magnitude as the photon energy increases, and finally peaks at the absorption edge of ~ 1.2 eV [Fig. 4(a)]. In the energy range from 1.4 to 3.0 eV, the real part of the $\chi_{aab}^{(2)}$ becomes positive and forms a broad double peak structure. Beyond 3.0 eV, it becomes negative again and its magnitude gradually diminishes as the photon energy further increases [Fig. 4(a)].

The absorptive part of the $\chi_{aab}^{(2)}$ is nonzero only above ~ 1.2 eV, and looks like a Lorentzian oscillation between 1.2 and 3.5 eV with one sharp negative peak at ~ 1.4 eV and one broad positive peak around 2.8 eV [Fig. 4(a)]. It is clear from Eqs. (2) and (3) that the calculated

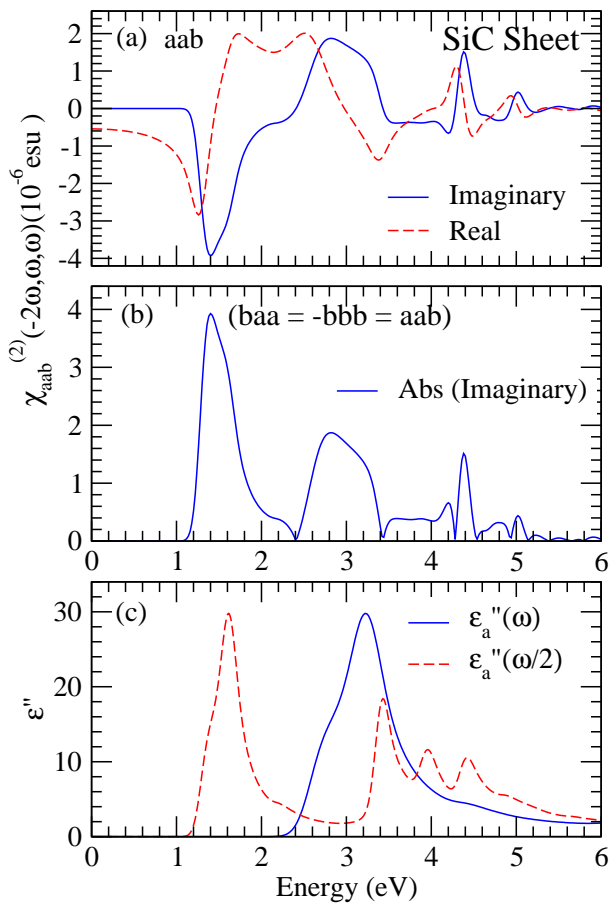


FIG. 4: (Color online) (a) Real and imaginary parts as well as (b) the absolute value of the imaginary part of $\chi_{aab}^{(2)}(-2\omega, \omega, \omega)$ of the isolated SiC sheet. In (c), $\varepsilon_a''(\omega)$ and $\varepsilon_a''(\omega/2)$ (imaginary part of the dielectric function) from Ref. [28] are plotted.

$\chi_{aab}^{(2)}$ spectra can have pronounced features due to both single- and double-frequency resonant terms. To analyze the features in the calculated $\chi^{(2)}$ spectra, it is helpful to compare the absolute value of $\chi''^{(2)}$ [Fig 4(b)] with the absorptive part of the corresponding dielectric function ε'' . Therefore, the calculated ε'' from our previous publication [28] are shown in Fig. 4(c) as a function of both $\omega/2$ and ω . Clearly, the first sharp peak at ~ 1.4 eV is due to two-photon resonances [cf. $\varepsilon_a''(\omega/2)$] while in contrast, the second broad peak around 2.8 eV comes from the single-photon resonances [cf. $\varepsilon_a''(\omega)$]. Nevertheless, both single- and double-photon resonances involve only interband $\pi \rightarrow \pi^*$ and $\sigma \rightarrow \sigma^*$ optical transitions for the electric field vector \mathbf{E} polarized parallel to the SiC layer ($E \parallel \hat{a}$) [28].

In Table II, the calculated zero frequency linear electro-optic coefficient $r(0)$ as well as the corresponding second-order nonlinear optical susceptibility $\chi^{(2)}(0, 0, 0)$ and the static refraction index $n(0)$ are listed. The refraction index $n(0)(= \sqrt{\varepsilon(0)})$ is derived from the calculated static dielectric constant $\varepsilon(0)$ which has been reported in our

recent publication [28]. Significantly, the linear electro-optical coefficients of the isolated SiC sheet are about ten times larger than that of the bulk SiC polytypes (Table II). The static second-order optical susceptibility for the SiC sheet is nearly six times larger than the largest component of $\chi^{(2)}(0, 0, 0)$ of the SiC polytypes. Furthermore, the zero frequency linear electro-optic coefficient $r(0)$ and the corresponding second-order nonlinear optical susceptibility $\chi^{(2)}(0, 0, 0)$ of the SiC sheet are more than five times larger than the corresponding values of the BN sheet [27].

C. Second-order optical susceptibility

We have explicitly calculated the second-order optical susceptibility for the zigzag (5,0), (6,0), (8,0), (9,0), (12,0), (16,0), (20,0), (24,0), armchair (3,3), (4,4), (5,5), (8,8), (12,12), (15,15), and chiral (4,2), (6,2), (8,4), (10,4) SiC-NTs. In the case of CNTs, only the chiral nanotubes would exhibit second-order nonlinear optical behavior with two nonvanishing components of xyz and xzy of $\chi^{(2)}$. [3] Here z refers to the coordinate along the tube axis while x and y denote the two coordinates that are perpendicular to the tube axis. As for CNTs, the armchair SiC-NTs are found not to have any nonzero components of $\chi^{(2)}$. In contrast, as in the case of the BN-NTs [27], both the zigzag and chiral SiC-NTs are found to show second-order nonlinear optical behavior. Specifically, all the zigzag SiC-NTs except (5,0), and (9,0), have six nonvanishing components of the second-order optical susceptibility, namely, xzx , xzx , yyz , zxx , zyy , zzz . Nevertheless, these components are not completely independent of each other. In particular, $\chi_{xzx}^{(2)} = \chi_{yyz}^{(2)} = \chi_{xzx}^{(2)}$, and $\chi_{zyy}^{(2)} = \chi_{zxx}^{(2)}$. The chiral SiC-NTs have eight nonvanishing components of the second-order optical susceptibility with two additional nonzero components being xyz and yzx . Note that $\chi_{yzx}^{(2)} = -\chi_{xyz}^{(2)}$. These numerical findings are consistent with the consideration of the symmetry of the SiC nanotubes. The point symmetry groups of the SiC-NTs [38] are C_{2nv} for zigzag ($n,0$) nanotubes, C_{2nh} for armchair (n,n) nanotubes, and C_N for chiral (n,m) nanotubes where $N = 2(n^2 + m^2 + nm)/d_R$ with d_R being the greatest common divisor of $2n+m$ and $2m+n$. Therefore, these symmetries would dictate [38] that all the components vanish for armchair (n,n) nanotubes, and that nonvanishing components for zigzag ($n,0$) nanotubes are $xzx = yzy$, $xzx = yzy$, $zxx = zyy$, zzz , as well as that nonvanishing components of chiral (n,m) nanotubes include all that for zigzag ($n,0$) nanotubes plus $xyz = -yzx$.

We display in Fig. 5 the calculated real and imaginary parts of the second-order optical susceptibility $\chi^{(2)}(-2\omega, \omega, \omega)$ for the four selected zigzag nanotubes [(6,0), (12,0), (20,0), and (24,0)]. As for the single SiC sheet, the second harmonic generation coefficients $\chi^{(2)}(-2\omega, \omega, \omega)$ for the zigzag SiC-NTs are significant in

TABLE III: Calculated second-order optical susceptibility $\chi^{(2)}(0)$ (pm/V) of the four SiC polytypes, together with other theoretical [Adolph *et al.* [39], Rashkeev *et al.* [41], Chen *et al.* [42]] and experimental [Lundquist *et al.* [43], Niedermeier *et al.* [44]] results.

	2H $\chi_{zzz}^{(2)}, \chi_{zxx}^{(2)}$	4H $\chi_{zzz}^{(2)}, \chi_{zxx}^{(2)}$	6H $\chi_{zzz}^{(2)}, \chi_{zxx}^{(2)}$	3C $\chi_{xyz}^{(2)}$
This work	11.5,-17.9	32.8,-20.4	38.6,-20.4	34.2
Adolph <i>et al.</i> [39]	4.5, -7.1	15.5, -9.7	18.1, -9.8	17.7
Rashkeev <i>et al.</i> [41]	3.6, -6.1	14.5, -8.9	17.8, -9.7	17.5
Chen <i>et al.</i> [42]	8.6, -13.2	23.3, -14.8	27.6, -15.0	24.4
Lundquist <i>et al.</i> [43]			86, -8.6	17.3
Niedermeier <i>et al.</i> [44]		18±8, -4±2	24±10, -4±2	

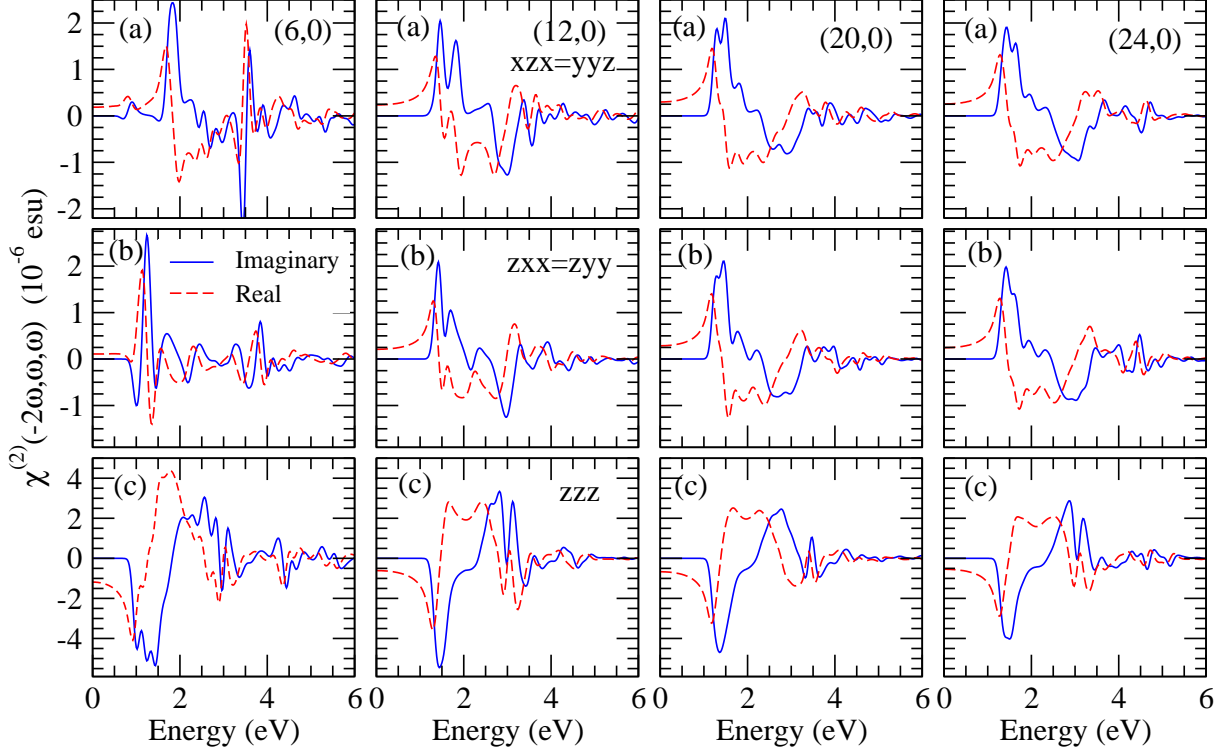


FIG. 5: (Color online) Real (dotted line) and imaginary parts (solid line) of $\chi^{(2)}(-2\omega, \omega, \omega)$ of the zigzag (6,0), (12,0), (20,0) and (24,0) SiC nanotubes.

the entire range of the optical photon energy ($\hbar\omega$). Indeed, they can be up to ten times larger than that of bulk SiC polytypes (see Figs. 1 and 5). Moreover, for the photon energy smaller than 2.0 eV, the $\chi^{(2)}$ is purely dispersive (i.e., real and lossless) (Fig. 5). Interestingly, the magnitude of $\chi_{zzz}^{(2)}$ is the largest (Fig. 5). For $\chi_{zzz}^{(2)}$, the electric field of both the incoming and outgoing photons is polarized parallel to the tube axis and thus the electric depolarization effect would be essentially zero (see Ref. 45 and references therein). This may be particularly important for nonlinear optical applications. The prominent features in each nonzero component of $\chi^{(2)}$ for all the zigzag SiC-NTs except the small-diameter (6,0) SiC-NT, look rather similar (Fig. 5). In particular, the spectra of the three xzx , zxx and zzz components of

$\chi^{(2)}$ for the (20,0) and (24,0) SiC-NTs are nearly identical (Fig. 5). We also note that the shape of the spectra of $\chi_{zzz}^{(2)}$ and $\chi_{zxx}^{(2)}$ for all the zigzag SiC-NTs look very similar, except the difference in sign. For the zigzag SiC-NTs with a larger diameter such as (12,0), (20,0) and (24,0), the spectrum of $\chi_{zxx}^{(2)}$ is also similar to that of $\chi_{zxx}^{(2)}$ (Fig. 5). The magnitude of the $\chi_{xzx}^{(2)}$ and $\chi_{zzz}^{(2)}$ components decreases slightly as the diameter of the tubes increases [e.g., from (6,0) to (24,0)], while the magnitude of the $\chi_{zxx}^{(2)}$ remains more or less independent of the diameter (Fig. 5). Furthermore, both the magnitude and shape of the $\chi_{zzz}^{(2)}$ spectrum for the zigzag SiC-NTs with a larger diameter, e.g., (20,0) and (24,0), approach to that of the single SiC sheet (Fig. 4), as they should.

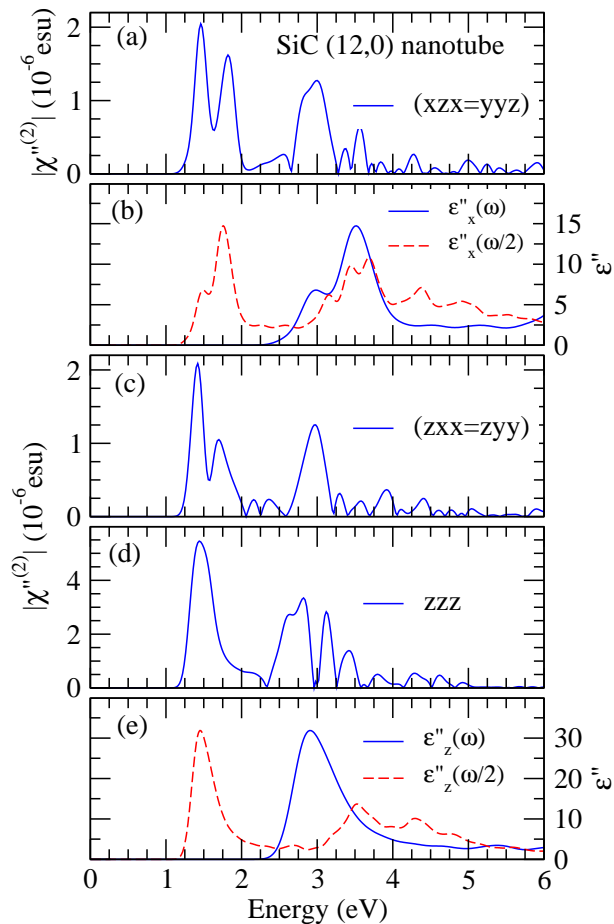


FIG. 6: (Color online) Absolute value of the imaginary part of $\chi^{(2)}(-2\omega, \omega, \omega)$ (a, c, d) as well as $\varepsilon''(\omega)$ and $\varepsilon''(\omega/2)$ (imaginary part of the dielectric function) (b, e) from Ref. [28] of the zigzag (12,0) SiC nanotube.

As for the single SiC sheet, in order to understand the features in the calculated $\chi^{(2)}$ spectra of the zigzag SiC-NTs, the absolute values of the imaginary part $\chi''^{(2)}$ of all the nonzero components of the (12,0) SiC-NT are plotted and compared with the absorptive part of the dielectric function ε'' from our previous publication [28] in Fig. 6. Strikingly, the first prominent peak between 1.0 and 2.0 eV in the $\chi''_{zzz}^{(2)}$ spectrum is almost identical to the first peak in the $\varepsilon''_z(\omega/2)$ (see Fig. 6(d) and 6(e)), indicating that it is due to two-photon resonances. In contrast, the second peak between 2.5 and 3.0 eV in the $\chi''_{zzz}^{(2)}$ spectrum is very similar to the first peak in the $\varepsilon''_z(\omega)$, suggesting that it is caused by the single-photon resonances. Nevertheless, both these single- and double-photon resonances involve only interband $\pi \rightarrow \pi^*$ and $\sigma \rightarrow \sigma^*$ optical transitions for the electric field vector \mathbf{E} polarized parallel to the tube axis ($E \parallel \hat{z}$) [28]. Fig. 6 also shows that the double-peak structure between 1.0 and 2.0 eV in both the $\chi''_{xzx}^{(2)}$ and $\chi''_{zxx}^{(2)}$ spectra is mainly due to the two-photon resonances with $E \perp \hat{z}$ [cf. $\varepsilon''_x(\omega/2)$] (see Fig. 6(a)-6(c)), while, in contrast, the second feature in the

photon energies above 3.0 eV perhaps comes predominantly from the single-photon resonances for $E \perp \hat{z}$ [cf. $\varepsilon''_x(\omega)$]. This conclusion is further supported by the fact that the magnitude of $\varepsilon''_x(\omega)$ ($\varepsilon''_x(\omega/2)$) is only about half of that of $\varepsilon''_z(\omega)$ ($\varepsilon''_z(\omega/2)$), and concurrently the magnitude of $\chi''_{xzx}^{(2)}$ and $\chi''_{zxx}^{(2)}$ is only about half of that of $\chi''_{zzz}^{(2)}$ too.

In Fig. 7, the calculated real and imaginary parts of the second-order optical susceptibility $\chi^{(2)}(-2\omega, \omega, \omega)$ for all the four chiral nanotubes [(4,2), (6,2), (8,4) and (10,4)] are displayed. In general, the spectra of each component of the second-order optical susceptibility for the chiral SiC-NTs with a moderate diameter [e.g., (8,4) and (10,4)] are similar. For all the chiral SiC-NTs except the ultra-small diameter (4,2) SiC-NT, remarkably, the zzz component is nearly four times larger than all the other nonvanishing components. Another common feature is that both the real and imaginary parts of $\chi^{(2)}(-2\omega, \omega, \omega)$ show a rather oscillatory behavior, particularly for the xyz and xzx components (Fig. 7). The amplitude of these oscillatory real and imaginary parts is rather large in the photon energies of 1.0~4.0 eV for the chiral SiC-NTs with a small diameter. It should also be noted that the shape and magnitude of the xzx and zxx components look very much alike (Fig. 7(b)-7(c)). Finally, both the magnitude and shape of the $\chi''_{zzz}^{(2)}$ spectrum for the chiral SiC-NTs with a larger diameter, e.g., (10,4), approach to that of the single SiC sheet (Fig. 4), as expected.

Again, in order to understand the structures in the calculated $\chi^{(2)}$ spectra of the chiral SiC-NTs, the absolute values of the imaginary part $\chi''^{(2)}$ of all the nonzero components of the (8,4) SiC-NT are plotted and compared with the absorptive part of the corresponding dielectric function ε'' from our previous publication [28] in Fig. 8. Remarkably, the first prominent peak between 1.0 and 2.0 eV in the $\chi''_{zzz}^{(2)}$ spectrum is almost identical to the first peak in the $\varepsilon''_z(\omega/2)$ (see Fig. 8(d)-8(e)), indicating that it is due to two-photon resonances. On the other hand, the second structure between 2.5 and 3.5 eV in the $\chi''_{zzz}^{(2)}$ spectrum may be correlated with the first peak in the $\varepsilon''_z(\omega)$, suggesting that it is caused by the single-photon resonances. As for the zigzag SiC-NTs, both these single-photon and double-photon resonances involve only interband $\pi \rightarrow \pi^*$ and $\sigma \rightarrow \sigma^*$ optical transitions for the electric field vector \mathbf{E} polarized parallel to the tube axis ($E \parallel \hat{z}$) [28]. Fig. 8 further suggests that the feature between 1.0 and 2.0 eV in the spectra of both the $\chi''_{xzx}^{(2)}$ and $\chi''_{zxx}^{(2)}$ as well as $\chi''_{xyz}^{(2)}$ may be attributed to the two-photon resonances with $E \perp \hat{z}$ [cf. $\varepsilon''_x(\omega/2)$] (see Fig. 8(a)-8(c)), while, in contrast, the second feature in the photon energies above 3.0 eV is mainly due to the single-photon resonances for $E \perp \hat{z}$ [cf. $\varepsilon''_x(\omega)$].

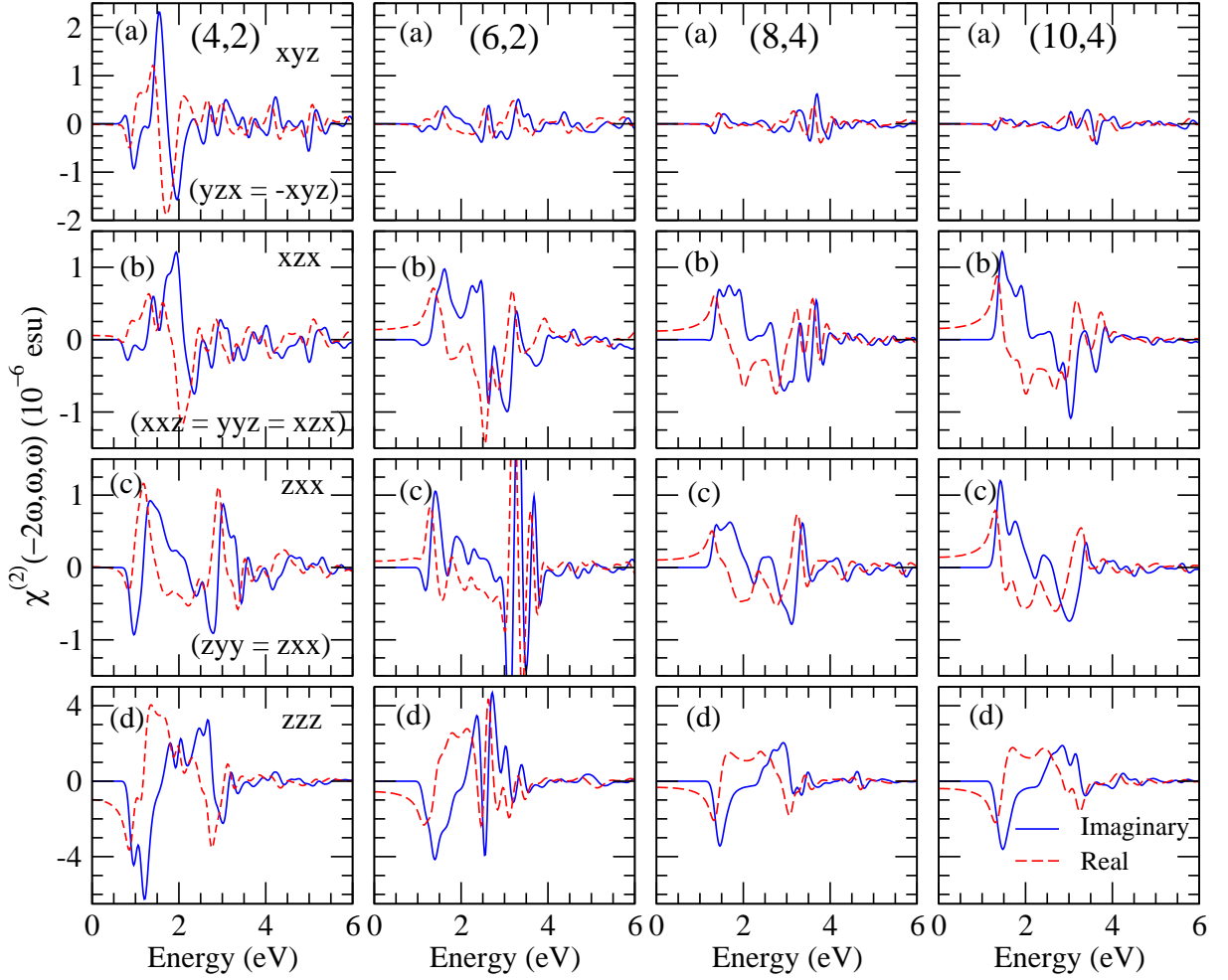


FIG. 7: (Color online) Real (dotted line) and imaginary parts (solid line) of $\chi^{(2)}(-2\omega, \omega, \omega)$ of the chiral (4,2), (6,2), (8,4) and (10,4) SiC nanotubes.

D. Linear electro-optical coefficient

We list in Table IV the calculated zero frequency linear electro-optic coefficient $r(0)$ as well as the corresponding second-order nonlinear optical susceptibility $\chi^{(2)}(0, 0, 0)$ of the SiC-NTs. The $r(0)$ is calculated from the corresponding $\chi^{(2)}(0, 0, 0)$ by using Eq. (7). The refraction index $n(0) (= \sqrt{\varepsilon(0)})$ is derived from the calculated static dielectric constant $\varepsilon(0)$ which has been reported in our recent publication [28]. Table IV shows that apart from the (5,0) and (9,0) SiC-NTs which have no non-vanishing $r_{abc}(0)$, and also the small diameter (6,0) and (8,0) SiC-NTs, all the other zigzag SiC-NTs have very similar linear electro-optical coefficients, as for the static dielectric constant and polarizability [28]. Nevertheless, $r_{zzz}(0)$ decreases slightly as the diameter increases, while $r_{xzx}(0)$ and $r_{zxx}(0)$ increase slightly as the diameter goes up. Remarkably, the static $\chi_{zzz}^{(2)}$ for the ultra-small diameter (6,0) is very large (Table IV), being nearly thirteen times larger than the largest component of $\chi^{(2)}$ of all the four bulk SiC polytypes (Table II). This suggests that

the SiC-NTs would be useful for applications in the non-linear optical devices. Nonetheless, the $\chi_{zzz}^{(2)}$ decreases rapidly as the diameter of the zigzag SiC-NTs increases, and, for the large diameter (24,0) SiC-NT, approaches the value of $\chi_{aab}^{(2)}$ of the single SiC sheet (Table II). The magnitude of the $\chi_{aab}^{(2)}$ is about half of the magnitude of the $\chi_{zzz}^{(2)}$ for the (6,0) SiC-NT. We note that $\chi_{xzx}^{(2)}$ and $\chi_{zxx}^{(2)}$ are rather similar, and their magnitudes increase as their tube diameters increases. Finally, for the larger diameter zigzag SiC-NTs, the $\chi_{zzz}^{(2)}$ is about two times larger than $\chi_{xzx}^{(2)}$ and $\chi_{zxx}^{(2)}$ (Table IV).

The chiral SiC-NTs have two additional nonvanishing components $\chi_{xyz}^{(2)}$ and $\chi_{yzx}^{(2)}$. Nevertheless, the calculated static values of $\chi_{xyz}^{(2)}$ and $\chi_{yzx}^{(2)}$ are negligibly small (i.e., within the numerical uncertainty), thereby satisfying the requirement by the so-called Kleinman symmetry [40] which demands that $\chi_{xyz}^{(2)}(0) = \chi_{yzx}^{(2)}(0)$. Consequently, the corresponding static linear electro-optical coefficients $r_{xyz}(0)$ and $r_{yzx}(0)$ are zero too. Therefore, $\chi_{yzx}^{(2)}$, $\chi_{xyz}^{(2)}$,

TABLE IV: Calculated static refraction index n , second-order optical susceptibility $\chi^{(2)}$ and linear electro-optical coefficient r_{abc} of the zigzag and chiral SiC nanotubes.

	n_x (n_z)	$\chi_{xxx}^{(2)}, \chi_{zxx}^{(2)}, \chi_{zzz}^{(2)}$ (pm/V)	$r_{xxz}, r_{zxx}, r_{zzz}$ (pm/V)
(5,0)	2.50 (3.39)	0.0, 0.0, 0.0	0.0, 0.0, 0.0
(6,0)	2.53 (3.31)	77.3, 45.5, -495.5	-2.19, -1.29, 8.21
(8,0)	2.56 (3.23)	87.6, 68.0, -323.1	-2.56, -1.98, 5.92
(9,0)	2.58 (3.23)	0.0, 0.0, 0.0	0.0, 0.0, 0.0
(12,0)	2.60 (3.21)	98.9, 88.1, -255.4	-2.84, -2.53, 4.82
(16,0)	2.62 (3.21)	104.7, 96.9, -241.9	-2.96, -2.74, 4.57
(20,0)	2.68 (3.27)	125.0, 119.6, -279.2	-3.25, -3.11, 4.85
(24,0)	2.63 (3.19)	107.1, 102.1, -227.7	-3.05, -2.91, 4.39
(4,2)	2.74 (3.37)	23.9, 4.46, -410.4	-0.56, -0.11, 6.36
(6,2)	2.56 (3.16)	58.2, 37.0, -236.6	-1.78, -1.13, 4.75
(8,4)	2.62 (3.17)	50.3, 43.6, -138.6	-1.46, -1.26, 2.75
(10,4)	2.62 (3.17)	65.3, 59.3, -164.3	-1.89, -1.72, 3.25

$r_{xyz}(0)$ and $r_{yzx}(0)$ for the chiral SiC-NTs are not listed in Table IV. As for the nonvanishing static components, $r_{zxx}(0)$ and $r_{zzz}(0)$ for the (6,2), (8,4) and (10,4) SiC-NTs are quite close. $\chi_{zzz}^{(2)}(0)$ and $r_{zzz}(0)$ decrease as the tube diameter increases, while, in contrast, $\chi_{zxx}^{(2)}(0)$ and $r_{zxx}(0)$ increase with the tube diameter. $r_{zxx}(0)$ and $r_{zzz}(0)$ for the (4,2) is somewhat smaller than that of the other chiral SiC-NTs.

The zero frequency second-order nonlinear optical susceptibility $\chi^{(2)}(0, 0, 0)$ of the SiC-NTs (Table IV) are generally a few times larger than the counterparts of the corresponding BN-NTs [27]. In particular, the $\chi_{zzz}^{(2)}(0, 0, 0)$ of the (6,0) SiC-NT is about thirteen times larger than that of the (6,0) BN-NT [27]. On the other hand, the $\chi_{zzz}^{(2)}(0, 0, 0)$ of the (24,0) SiC-NT is only about six times larger than that of the (24,0) BN-NT [27]. This suggests that compared with BN-NTs, SiC-NTs would be a better nonlinear optical material. However, the low frequency linear electro-optic coefficient $r(0)$ of the SiC-NTs (Table IV) are only slightly larger than the counterparts of the corresponding BN-NTs [27]. For example, the $r_{zzz}(0)$ of the (6,0) and (24,0) SiC-NTs is, respectively, 1.7 and 1.3 times larger than that of the (6,0) and (24,0) BN-NTs. This is because the refraction index n of the SiC-NTs (Table IV) are also larger than that of the BN-NTs [27] [see Eq. (7)].

IV. SUMMARY

We have carried out a systematic *ab initio* study of the second-order nonlinear optical properties of SiC-NTs within density functional theory in the local density approximation. We used the highly accurate full-potential PAW method. The underlying atomic structure of the SiC nanotubes was determined theoretically. Specifically, the properties of the single-walled zigzag [(5,0),

(6,0), (8,0), (9,0), (12,0), (16,0), (20,0), (24,0)], armchair [(4,4), (5,5), (8,8), (12,12), (15,15)], and chiral [(4,2), (6,2), (8,4), (10,4)] nanotubes have been calculated. For comparison, the second-order nonlinear optical properties of bulk SiC polytypes (2H-, 4H-, 6H- and 3C-SiC) and the single graphitic SiC sheet have also been calculated. Interestingly, we find that the $\chi_{aab}^{(2)}$, $\chi_{baa}^{(2)}$ and $\chi_{bbb}^{(2)}$ for the isolated SiC sheet are large and generally several times larger than that of the SiC polytypes. Unlike carbon nanotubes, both the chiral and zigzag SiC-NTs have pronounced second-harmonic generation and linear electro-optical coefficients which are comparable to or even larger than that of the single SiC sheet. The prominent structures in the spectra of $\chi^{(2)}(-2\omega, \omega, \omega)$ of the SiC-NTs have been related to the features in the corresponding linear optical dielectric function $\varepsilon(\omega)$ in terms of single-photon and double-photon resonances. We also find that the $\chi_{abc}^{(2)}$ and r_{abc} coefficients of the SiC-NTs are up to thirteen-times larger than the counterparts of the corresponding BN-NTs. Therefore, the SiC-NTs would be promising nonlinear optical materials for applications in, e.g., second-harmonic generation, sum frequency generation and electro-optical switches. We hope that this work would stimulate experimental investigations into the second-order nonlinear optical properties of the SiC-NTs.

V. ACKNOWLEDGMENTS

The authors gratefully acknowledge financial support from National Science Council and NCTS of ROC. The author also thank the National Center for High-Performance Computing of ROC, and the Computer and Information Networking Center (CINC) of National Taiwan University for providing CPU time.

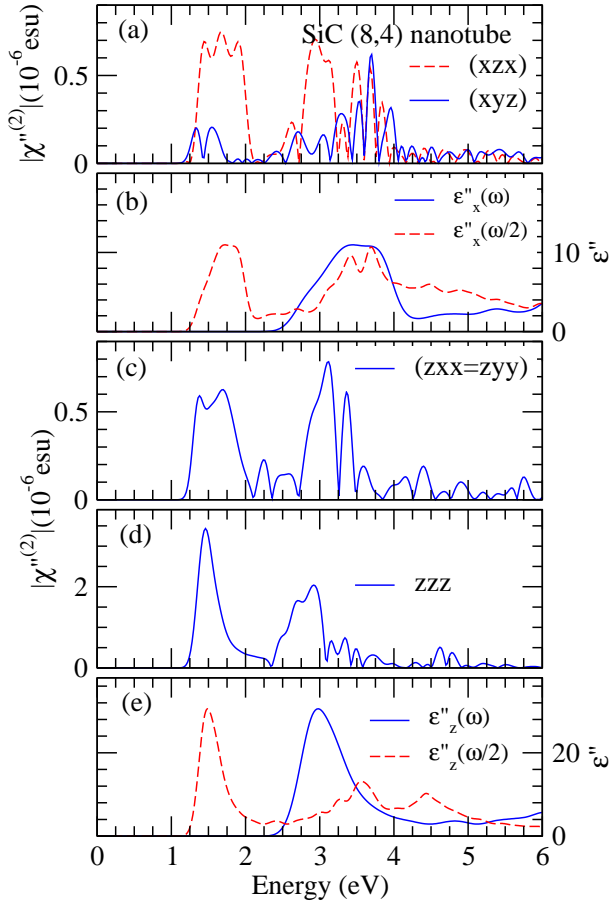


FIG. 8: (Color online) Absolute value of the imaginary part of $\chi^{(2)}(-2\omega, \omega, \omega)$ (a, c, d) and $\epsilon''(\omega)$ and $\epsilon''(\omega/2)$ (imaginary part of the dielectric function) (b, e) from Ref. [28] of the zigzag (8,4) SiC nanotube.

-
- [1] S. Iijima, *Nature (London)* **354**, 56 (1991).
- [2] R. Saito, G. Dresselhaus, and M. S. Dresselhaus, *Physical properties of Carbon Nanotubes* (Imperial College, London, 1998).
- [3] G. Y. Guo, K. C. Chu, D.-S. Wang, and C.-G. Duan, *Phys. Rev. B* **69**, 205416 (2004).
- [4] G. Y. Guo, K. C. Chu, D.-S. Wang, and C.-G. Duan, *Comp. Mater. Sci.* **30**, 269 (2004).
- [5] A. Rubio, J. L. Corkill, and M. L. Cohen, *Phys. Rev. B* **49**, R5801 (1994).
- [6] N. G. Chopra, R. J. Luyken, K. Cherry, V. H. Crespi, M. L. Cohen, S. G. Louie, and A. Zettle, *Science* **28**, 335 (1994).
- [7] M. Zhao, Y. Y. Xia, D. J. Zhang and L. M. Mei, *Phys. Rev. B* **68**, 235415 (2003).
- [8] S. M. Lee, Y. H. Lee, Y. G. Hwang, J. Elsner, D. Porezag, and Th. Frauenheim, *Phys. Rev. B* **60**, 7788 (1999).
- [9] *Semiconductors: Physics of Group IV Elements and III-V Compounds*, edited by K.-H. Hellwege and O. Madelung, Landolt-Börnstein, New Series, Group III, Vol. 17, Pt. a (Springer-Verlag, Berlin, 1982).
- [10] R. W. G. Wyckoff, *Crystal Structures* (Wiley, New York, 1963).
- [11] P. A. Ivanov and V. E. Chelnokov, *Semicond. Sci. Technol.* **7**, 863 (1992).
- [12] C. Persson and U. Lindefelt, *J. App. Phys.* **82**, 5496, (1997)
- [13] R. Wang, D. Zhang, C. Liu, *Chemical Phys. Lett.* **411**, 333, (2005).
- [14] R. Rurali, P. Godignon, J. Rebollo, E. Hernandez, and P. Ordejon, *Appl. Phys. Lett.* **82**, 4298 (2003).
- [15] C. H. Park, B. H. Cheong, K. H. Lee, and K.J. Chang, *Phys. Rev. B* **49**, 4485, (1994)
- [16] *Properties of Silicon Carbide*, edited by G. L. Harris (INSPEC, Institution of Electrical Engineers, London, 1995)
- [17] X.-H. Sun, C.-P. Li, W.-K. Wong, N.-B. Wong, C.-S. Lee, S.-T. Lee, and B.-K. Teo, *J. Am. Chem. Soc.* **124**, 14464 (2002).
- [18] L. Z. Pei, Y. H. Tang, Y. W. Chen, C. Guo, X. X. Li, Y. Yuan, and Y. Zhang, *J. Appl. Phys.* **99**, 114306 (2006).
- [19] L. Z. Pei, Y. H. Tang, X. Q. Zhao, Y. W. Chen and C. Guo, *J. App. Phys.* **100**, 046105 (2006).

- [20] M. Menon, E. Richter, A. Mavrandonakis, G. Froudakis, and A. N. Andriotis, Phys. Rev. B **69**, 115322 (2004).
- [21] M. Zhao, Y. Xia, F. Li, R. Q. Zhang and S. T. Lee, Phys. Rev. B **71**, 085312 (2005).
- [22] A. Mavrandonakis, G. E. Froudakis, M. Schnell, and Muhlhauser, Nano Lett. **3**, 1481 (2004).
- [23] Y. Miyamoto and B. D. Yu, Appl. Phys. Lett. **80**, 586 (2002).
- [24] M. Zhao, Y. Xia, R. Q. Zhang, and S. T. Lee, J. Chem. Phys. **122**, 214707 (2005).
- [25] A. Gali, Phys. Rev. B **73**, 245415 (2006).
- [26] S. M. Nakhmanson, A. Calzolari, V. Meunier, J. Bernholc, and M. B. Nardelli, Phys. Rev. B **67**, 235406 (2003).
- [27] G. Y. Guo, and J. C. Lin, Phys. Rev. B **72**, 075416 (2005); *ibid* **77**, 049901(E) (2008).
- [28] I. J. Wu, and G. Y. Guo, Phys. Rev. B **76**, 035343 (2007).
- [29] P. E. Blöchl, Phys. Rev. B **50**, 17953 (1994); G. Kresse and D. Joubert, *ibid.* **59**, 1758 (1999).
- [30] G. Kresse and J. Hafner, Phys. Rev. B **47**, R558 (1993); **49**, 14251 (1994); G. Kresse and J. Furthmüller, Comput. Mater. Sci. **6**, 15 (1996).
- [31] C.-G. Duan, J. Li, Z.-Q. Gu, and D.-S. Wang, Phys. Rev. B **60**, 9435 (1999).
- [32] Ed. Ghahramani, D.J. Moss and J.E. Sipe, Phys. Rev. Lett. **64**, 2815 (1990); *ibid*, Phys. Rev. B **43**, 8990 (1991).
- [33] B. Adolph, J. Furthmüller, and F. Bechstedt, Phys. Rev. B **63**, 125108 (2001).
- [34] J. L. P. Hughes, and J. E. Sipe, Phys. Rev. B **53**, 10751 (1996).
- [35] N. W. Jepps, and T. F. Page, Progr. Cryst. Growth Charact. **7**, 259 (1983).
- [36] F. Bechstedt, P. Käckell, A. Zywietz, K. Karch, B. Adolph, K. Tenelsten, and J. Furthmüller, Phys. Stat. Sol. (b) **202**, 35 (1997).
- [37] B. Wenzien, P. Käckell, F. Bechstedt, and G. Cappellini, Phys. Rev. B **52**, 10897 (1995).
- [38] R. W. Boyd, *Nonlinear Optics* (Elsevier, Amsterdam, 2003).
- [39] B. Adolph, and F. Bechstedt, Phys. Rev. B **62**, 1706 (2000).
- [40] D. A. Kleinmam, Phys. Rev. **126**, 1977 (1962).
- [41] S. N. Rashkeev, W. R. L. Lambrecht, and B. Segall, Phys. Rev. B **57**, 9705 (1998).
- [42] J. Chen, Z. H. Levine, and J. W. Wilkins, Phys. Rev. B **50**, 11514 (1994).
- [43] P. M. Lundquist, W. P. Lin, G. K. Wong, M. Razeghi, and J. B. Ketterson App. Phys. Lett. **66**, 1883 (1995).
- [44] S. Niedermeier, H. Schillinger, R. Sauerbrey, B. Adolph, and F. Bechstedt, App. Phys. Lett. **75**, 618 (1999).
- [45] G. Y. Guo, S. Ishibashi, T. Tamura and K. Terakura, Phys. Rev. B **75**, 245403 (2007).